This is the peer reviewd version of the followng article:

Dual series solution for the standardized ISRM Brazilian disc test modelled as an advancing contact problem / Radi, E.. - In: INTERNATIONAL JOURNAL OF ROCK MECHANICS AND MINING SCIENCES. - ISSN 1365-1609. - 173:(2024), pp. 1-11. [10.1016/j.ijrmms.2023.105634]

Terms of use:

The terms and conditions for the reuse of this version of the manuscript are specified in the publishing policy. For all terms of use and more information see the publisher's website.

14/11/2026 14:00

(Article begins on next page)

International Journal of Rock Mechanics and Mining Sciences xxx (xxxx) 105634



Contents lists available at ScienceDirect

International Journal of Rock Mechanics and Mining Sciences

journal homepage: www.elsevier.com/locate/ijrmms



Dual series solution for the standardized ISRM Brazilian disc test modelled as an advancing contact problem

E. Radi

Dipartimento di Scienze e Metodi dell'Ingegneria, Università di Modena e Reggio Emilia, Via G. Amendola 2, I-42122, Reggio Emilia, Italy

ARTICLE INFO

Keywords:
Brazilian disc test
Advancing contact
Dual trigonometric series
Contact pressure
Linear elasticity

ABSTRACT

A new analytical solution is found for the stress and displacement fields in a standardized ISRM Brazilian disc test with curved jaws, based on the solution of a set of dual trigonometric series. The disc is assumed to be linear elastic and isotropic and in frictionless advancing contact with the two jaws assumed as rigid, under plane stress loading conditions. Use is made of the Michell solution for an elastic disc in polar coordinates, whose coefficients are found by imposing the mixed boundary conditions along the disc rim, both along the free surface and the contact region. The problem is first reduced to a set of dual trigonometric series and then to a linear system of infinite equations, which is solved by truncation. The non-linear relations providing the contact angular extent and pressure distribution in terms of the applied load or jaw displacement, consequent to the progressive advance of the contact, are derived by using an inverse method. The obtained results are validated by comparison with previous theoretical and experimental results available in the literature. The study indicates that the method of dual series is simpler and more straightforward as compared to the analytical methods proposed in the literature for treating the Brazil disc test as an advancing contact problem.

UNCORRECTED PROOF

1. Introduction

The Brazilian disc test is widely employed for indirectly measuring the tensile strength of brittle materials, like rocks and concrete, as an alternative to unpractical direct tensile tests. The specifications for the testing procedure and apparatus were established by the America Society for Testing and Materials (ASTM) and by the International Society for Rock Mechanics (ISRM),[1] independently. A comprehensive review of the literature related to the Brazilian disc test can be found in Ref. 2. In a standardized Brazilian disc test, a non-linear variation of the stress field is expected as the load is increased also for linear elastic behavior of the material, due to the progressive expansion of the contact region with the amount of loading. Consequently, the failure load is expected to depend on the size of the contact zone. In spite of this, most of the analytical and numerical investigations of the problem available in the literature assume a specific distribution of the contact pressure and do not take into account the increase in the contact length with the load.[3–7] By assuming uniform pressure distribution, Hondros[4] derived a relation between the maximum principal stress at the centre of the disc and the applied load and contact angle. Since it is very difficult to measure the latter parameter accurately during the test, it follows that the proposed relation is useful only in the limit as the contact angle tends to zero. In this case, the solution for a disc loaded by two opposite concentrated loads is recovered.[3,6] The validity of the Brazilian test for brittle materials was soon questioned in Ref. 5, pointing out that for small contact angles crack may initiate from the loading contact region instead of the centre of the test disc.

A number of studies examined the effect of the contact length by assuming a prescribed distribution of the radial pressure along the loaded rim, usually uniform, parabolic, sinusoidal, circular or elliptical.[7–14] However, if the increase in the contact length is neglected, then the tensile strength of the material provided by the Brazilian disc test is overestimated, especially for more compliant materials. In few analyses only, the Brazilian disc test is properly treated as an advancing contact problem. Assuming a very small length of the contact region, in Refs. 15–17 the disc-jaw system is approximated as two elastic half-planes in simple contact compressed against each other, whose contact rim is determined analytically by using the complex potentials method developed in Ref. 3. The corresponding analytical results are then validated by comparison with the experimental data obtained by using the Digital Image Correlation (DIC) technique. In these studies, the extent of the contact rim is found to have a limited influence on the stress field at the centre of the disc, while it has a strong influence on the stress field in proximity of the disc-jaw interface, where brittle fracture may occur due to stress concentration. In this case, the results of the Brazilian disc test do not provide the actual tensile strength of the disc material. As

E-mail address: enrico.radi@unimore.it.

https://doi.org/10.1016/j.ijrmms.2023.105634
Received 27 April 2023; Received in revised form 28 August 2023; Accepted 23 December 2023
1365-1609/© 20XX

Note: Low-resolution images were used to create this PDF. The original images will be used in the final composition.

observed in Ref. 8 and,[18] the location of the failure initiation moves from the loaded rim to the disc centre as the contact length increases. It follows that the knowledge of the actual contact length as a function of the applied load level and of geometrical and material parameters is mandatory for a reliable and accurate definition of the tensile strength of brittle materials by means of the Brazilian disc test. In particular, the increase in the contact length due to the adoption of curved jaws reduces the local damage due to the concentration of the contact pressure near the loaded rim and thus improves the reliability of the Brazilian test for measuring the tensile strength of the disc material.

Nowadays, advancing contact problems are still challenging.[19] They are usually treated by special numerical techniques, also for linear elastic behavior of the material, and only few analytical studies are available in the literature. Within this context, the advancing contact problem of a circular pin in a hole in an infinite elastic medium has been investigated analytically and numerically.[20–23] Recently, the advancing contact problem for a curved elastic beam indented by a rigid pin was investigated in Ref. 24 by using a fully analytical approach based on dual trigonometric series.

In the present work, the progressive contact between jaws and disc occurring in a standardized ISRM Brazilian disc test is modelled analytically, without any preliminary assumption on the contact pressure distribution. A new full-field analytical solution is obtained based on the dual series approach previously employed for modeling advancing contact problems between a rigid pin and an elastic curved beam,[24] between an incomplete elastic ring and a rigid plane,[25] and for a circular pin in a hole in an infinite medium.[26] This approach has never been proposed for the analysis of the Brazilian disc test before. Here, the stress and displacement fields are assumed in the form of a Michell-type series solution for a disc, whose coefficients are determined by imposing the vanishing of tractions along the free rim of the disc and the frictionless contact conditions along the rim in contact with the jaws. The problem is first reduced to a set of dual trigonometric series and then to a linear system of infinite equations, which is solved by truncation. Since the contact angular extent is unknown aforehand, the non-linear relationships for the contact angular extent and pressure distribution in terms of the applied load or jaw displacement, consequent to the progressive advance of the contact rim, are derived by using an inverse method. Specifically, the contact angular extent is assigned in advance and the corresponding stress field and total applied load are then calculated, for increasing values of the contact length.

The present approach also holds for a large contact angle as a difference to the complex potential method adopted in Refs. 15–17, which also assumes advancing contact between disc and jaws, but is based on the crucial assumption that the contact arc is very small compared to the dimensions of the disc and the jaw.

In the present analysis, the jaw displacement is assumed much smaller than the disc radius, according to the usual hypothesis of the linear elasticity theory. Moreover, the simplifying assumption of rigid behavior is adopted for the jaws, since the deformability of the disc materials, like rocks and concrete, is usually much larger than that of the metallic jaws. This assumption provides accurate results if the elastic modulus of the jaw exceeds ten times that of the disc.[27] For stiffer discs, the present approach is reasonably expected to underestimate the contact extent.

Finally, the analytical results here obtained are compared with FEM predictions and experimental data available in the literature and a reasonable agreement is observed for a broad level of loading.

2. Problem formulation

We consider the problem of an elastic circular disc of radius R pressed by two rigid jaws of curvature radius R_0 (Fig. 1), under plane stress loading conditions, where $R_0 = 1.5\,R$ according to the testing apparatus proposed by ISRM.[1] Due to the different curvature of the surfaces in contact, the extent of the contact region between the two components increases with increasing load P applied to the jaws and is not know in advance. Therefore, for this advancing contact problem the stress field in the disc is a nonlinear function of the applied load P or jaw displacement δ, whose solution depends on the geometry and mechanical properties of disc and jaws and is obtained in the following by using an inverse procedure. Namely, by assigning in advance the contact half-angle α and finding the corresponding stress and displacement fields. Then, the corresponding load P is calculated by integrating the contact pressure along the contact rim.

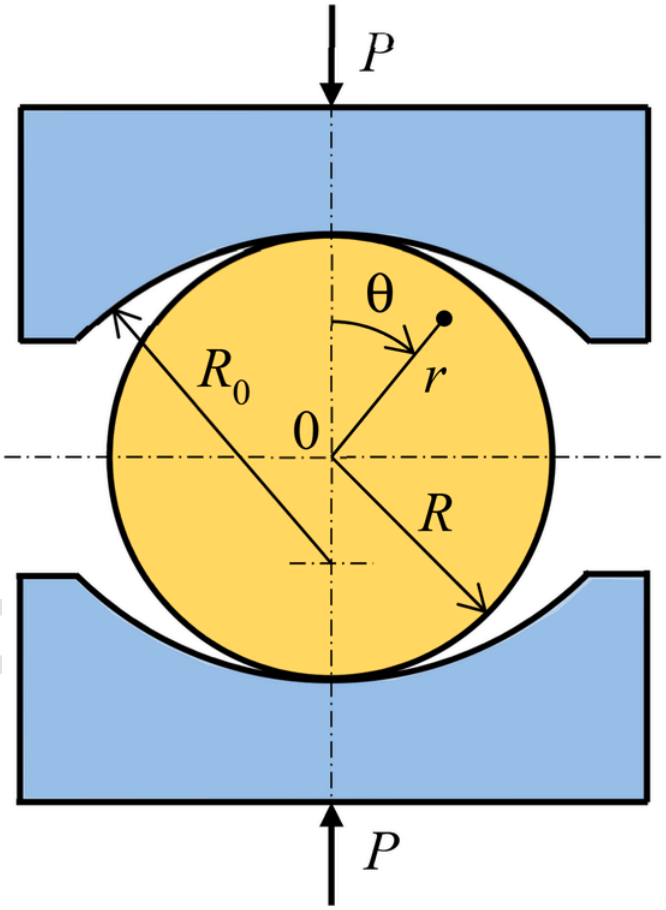


Fig. 1. Brazilian disc test according to the ISRM standard.

Reference is made to a polar coordinate system $(0, r, \theta)$ whose origin is taken at the disc centre, with the polar axis $\theta = 0$ along the direction of the applied load P (Fig. 1). Because of the symmetry, reference is made to a quarter of disc defined by the angular coordinate $0 \le \theta \le \pi/2$.

The mixed boundary conditions require the vanishing of shear tractions along the full disc rim, namely

$$\sigma_{r\theta} = 0, \qquad \text{for} \quad 0 \le |\theta| \le \pi/2, \quad r = R, \tag{2.1}$$

also due to the frictionless contact assumption. Moreover, the following conditions on the vanishing of the normal traction on the disc rim out of the contact region and on the radial displacement are enforced along the disc rim in contact with the jaw, namely

$$\begin{aligned} &\sigma_{rr} = 0, \qquad \text{for} \quad \alpha \le |\theta| \le \pi/2, \quad r = R, \\ &u_r = -\delta\cos\theta + (R_0 - R)\,(1 - \cos\theta), \qquad \text{for} \quad 0 \le |\theta| \le \alpha, \quad r = R, \end{aligned} \tag{2.2}$$

where α is the half contact angular extent and δ is the rigid body displacement of the jaw along the loading direction, which is assumed much smaller than the disc radius R. The contact condition $(2.2)_2$ on the

radial displacement along the contact zone was obtained in Refs. 20,28,29 for the almost conforming contact problem of a cylindrical pin in a hole, under the assumption that the pin displacement is much smaller than its radius. Contact conditions different from $(2.2)_2$ are instead considered in Ref. 27, where the rim displacement is assumed to occur only along the radial direction, and in Ref. 16, where the displacements of the two surface in contact is taken along the loading direction. An accurate derivation of condition $(2.2)_2$ together with the underlying hypothesis can be found in the Appendix, where the exact non-conformal contact condition is also derived.

The stress and displacement fields are taken as suggested by the Michell solution of the biharmonic equation in polar coordinates for a disc[12,30] under symmetric loading condition with respect to the axes $\theta = 0$ and $\theta = \pi/2$, namely

$$\begin{aligned}
\frac{\sigma_{rr}(r,\theta)}{2\mu} &= -\frac{A_0}{2} - \sum_{n=1}^{\infty}\left[n\,A_n\left(\frac{r}{R}\right)^{2(n-1)} - (n-1)\,B_n\left(\frac{r}{R}\right)^{2n}\right]\cos 2n\theta,\\
\frac{\sigma_{\theta\theta}(r,\theta)}{2\mu} &= -\frac{A_0}{2} + \sum_{n=1}^{\infty}\left[n\,A_n\left(\frac{r}{R}\right)^{2(n-1)} - (n+1)\,B_n\left(\frac{r}{R}\right)^{2n}\right]\cos 2n\theta,\\
\frac{\sigma_{r\theta}(r,\theta)}{2\mu} &= \sum_{n=1}^{\infty} n\left[A_n\left(\frac{r}{R}\right)^{2(n-1)} - B_n\left(\frac{r}{R}\right)^{2n}\right]\sin 2n\theta,
\end{aligned} \tag{2.3}$$

$$\begin{aligned}
\frac{u_r}{R} &= -\frac{\kappa-1}{4}\frac{r}{R}A_o - \sum_{n=1}^{\infty}\left[\frac{n\,A_n}{2n-1}\left(\frac{r}{R}\right)^{2n-1} - \frac{2n+1-\kappa}{2\,(2n+1)}\,B_n\left(\frac{r}{R}\right)^{2n+1}\right]\cos 2n\theta,\\
\frac{u_\theta}{R} &= \sum_{n=1}^{\infty}\left[\frac{n\,A_n}{2n-1}\left(\frac{r}{R}\right)^{2n-1} - \frac{2n+1+\kappa}{2\,(2n+1)}\,B_n\left(\frac{r}{R}\right)^{2n+1}\right]\sin 2n\theta,
\end{aligned} \tag{2.4}$$

where A_0, A_n, and B_n are arbitrary constants to be determined from the boundary conditions (2.2), μ is the elastic shear modulus of the disc and $\kappa > 1$ is the Kolosov constant,[30] namely

$$\kappa = \begin{cases} 3-4\nu & \text{for plane strain,}\\ \frac{3-\nu}{1+\nu} & \text{for plane stress.}\end{cases} \tag{2.5}$$

being ν the Poisson's ratio of the material.

The boundary condition (2.1) on the vanishing of the shear tractions along the full disc rim then yields the following relation between constants A_n and B_n,

$$A_n = B_n, \text{ for } n = 1, 2, \ldots \tag{2.6}$$

The mixed boundary conditions on the radial tractions and displacement (2.2) then provide a set of dual series equations for the unknown constants A_n $(n = 0, 1, 2, \ldots)$

$$\frac{A_0}{2} + \sum_{n=1}^{\infty} A_n \cos 2n\theta = 0, \quad \text{for } \alpha \le |\theta| \le \pi/2, \tag{2.7}$$

$$\begin{aligned}
&\frac{\kappa-1}{4}A_0 + \sum_{n=1}^{\infty}\left(\frac{1}{2n-1} + \frac{\kappa}{2n+1}\right)\frac{A_n}{2}\cos 2n\theta = \frac{\delta}{R}\cos\theta\\
&\quad - \frac{1-\rho}{\rho}(1-\cos\theta), \quad \text{for} \quad 0 \le |\theta| \le \alpha.
\end{aligned} \tag{2.8}$$

where $\rho = R/R_0 = 2/3$ for the ISRM standardized Brazil disc test and the angular contact extent α is unknown.

3. Solution of the dual series equations

As proposed in Ref. 31, the integrodifferential operator $(D + D^{-1})$ is applied on equation (2.8) to remove the unknown rigid body displacement δ, where

$$D\varphi = \frac{d\varphi}{d\theta}, \qquad D^{-1}\varphi = \int_0^{\theta} \varphi(s)\ ds, \tag{3.1}$$

Then, it follows

$$\begin{aligned}
&\left(\frac{\kappa-1}{4}A_0 + \frac{1-\rho}{\rho}\right)\theta = \sum_{n=1}^{\infty} A_n\left(\frac{1}{2n-1} + \frac{\kappa}{2n+1}\right)\frac{4n^2-1}{4n}\\
&\quad \sin 2n\theta, \quad \text{for} \quad 0 \le |\theta| \le \alpha.
\end{aligned} \tag{3.2}$$

By substituting $t = 2\theta$ in eqns (2.7) and (3).2), and multiplying the latter by $2/(1-\kappa)$, one obtains the following dual trigonometric series

$$\frac{A_0}{2} + \sum_{n=1}^{\infty} A_n \cos nt = 0, \ \text{for } 2\alpha \le |t| \le \pi, \tag{3.3}$$

$$\sum_{n=1}^{\infty} A_n \sin nt = (cA_0 + d)t + \sum_{n=1}^{\infty} h_n A_n \sin nt, \quad \text{for} \quad 0 \le |t| \le 2\alpha, \tag{3.4}$$

where

$$\begin{aligned}
c &= \frac{\kappa-1}{4(1+\kappa)},\\
d &= \frac{1-\rho}{\rho\,(1+\kappa)},\\
h_n &= 1 - \frac{2}{1+\kappa}\left(\frac{1}{2n-1} + \frac{\kappa}{2n+1}\right)\left(n - \frac{1}{4n}\right),
\end{aligned} \tag{3.5}$$

so that $h_n \to 0$ as $n \to \infty$

As proposed in Ref. 32, later adopted in Ref. 25, and recently in Ref. 24 to solve dual trigonometric series similar to eqns (3.3) and (3).4), an auxiliary stress function φ is introduced such that

$$\frac{A_0}{2} + \sum_{n=1}^{\infty} A_n \cos nt = H(2\alpha - t)\ \cos\frac{nt}{2}\int_0^{2\alpha}\frac{\varphi(s)\ ds}{\sqrt{\cos nt - \cos ns}}, \ \text{for } 0 \le |t| \le \pi, \tag{3.6}$$

where H denotes the Heavyside function. Then, as illustrated in Refs. 24,25, the coefficients A_n, for $n \ge 0$ of the Fourier cosine series expansion (3.6) are:

$$A_0 = \sqrt{2}\int_0^{2\alpha} \varphi(s)\, ds, \tag{3.7}$$

$$A_n = \frac{1}{\sqrt{2}}\int_0^{2\alpha}\left[P_n(\cos s) + P_{n-1}(\cos s)\right]\varphi(s)\, ds, \quad \text{for} \quad n \ge 1, \tag{3.8}$$

where P_n denotes the Legendre polynomials of order n. The introduction of (3.8) in eqn (3.4), using eqn (2.6).31 in Ref. 33, namely

$$\begin{aligned}
&\frac{1}{\sqrt{2}}\sum_{n=1}^{\infty}\left[P_n(\cos s) + P_{n-1}(\cos s)\right]\sin nt\\
&= \frac{H(t-s)\ \cos(t/2)}{\sqrt{\cos s - \cos t}},
\end{aligned} \tag{3.9}$$

then yields the following integral equation of the Abel type for the auxiliary stress function $\varphi(s)$

$$\int_0^t \frac{\varphi(s)\ ds}{\sqrt{\cos s - \cos t}} = \frac{1}{\cos(t/2)}\left[(cA_0 + d)t + \sum_{n=1}^{\infty} h_n A_n \sin nt\right], \ \text{for } 0 \le |t| \le 2\alpha, \tag{3.10}$$

which can be solved for $\varphi(s)$:

$$\begin{aligned}
\varphi(s) = \frac{2}{\pi}\frac{d}{ds}\int_0^s \Bigg[&\left(cA_0 + d\right)t\\
&+ \sum_{n=1}^{\infty} h_n A_n \sin nt\Bigg]\frac{\sin(t/2)\ dt}{\sqrt{\cos t - \cos s}}.
\end{aligned} \tag{3.11}$$

Using the results

$$\begin{aligned}
&\int_0^s \frac{t\ \sin(t/2)}{\sqrt{\cos t - \cos s}}dt = -\sqrt{2}\pi\ \ln\left(\cos\frac{s}{2}\right),\\
&\int_0^s \frac{\sin nt\ \sin(t/2)}{\sqrt{\cos t - \cos s}}dt = -\frac{\pi}{2\sqrt{2}}\left[P_n(\cos s) - P_{n-1}(\cos s)\right],
\end{aligned} \tag{3.12}$$

provided in the appendix of[26] and in Ref. 33, respectively, the integrals in eqn (3.11) can be calculated in closed form, thus obtaining

CORRECTED PROOF

$$\varphi(s) = \frac{1}{\sqrt{2}} \left\{ 2\left(cA_0 + d\right) + \sum_{n=1}^{\infty} nh_n A_n \left[P_n(\cos s) + P_{n-1}(\cos s)\right] \right\} \tan\frac{s}{2}. \tag{3.13}$$

The introduction of eqn (3.13) in (3.7) and (3.8), choosing a finite number of terms N in the sum, then gives the following linear system of algebraic equations for the unknown coefficients A_n, for $n = 0, 1, \ldots, N$:

$$A_0 = -4\left(cA_0 + d\right) \ln(\cos\alpha) + \sum_{n=1}^{N} nh_n A_n H_n, \tag{3.14}$$

$$A_n = \left(cA_0 + d\right) H_n + \sum_{m=1}^{N} \frac{m}{2} K_{nm} h_m A_m, \quad \text{for } n = 1, \ldots, N, \tag{3.15}$$

where

$$H_n = \frac{P_{n-1}(\cos 2\alpha) - P_n(\cos 2\alpha)}{n}, \tag{3.16}$$

$$K_{nm} = \frac{(1+\cos 2\alpha)(\sin 2\alpha)^2}{2\left(n^2 - m^2\right)} \times \left[(n+1) P_{m-1}^{(0,1)}(\cos 2\alpha) P_{n-2}^{(1,2)}(\cos 2\alpha) - (m+1) P_{n-1}^{(0,1)}(\cos 2\alpha) P_{m-2}^{(1,2)}(\cos 2\alpha)\right], \tag{3.17}$$

and $P_n^{(a,b)}(t)$ denotes the Jacobi polynomials of order n and $H_n \to 0$ as $n \to \infty$. A detailed derivation of the results (3.16) and (3.17) can be found in Ref. 24, where the coefficient K_{nm} for $n = m$ is also calculated as a limit.

Once the first $N+1$ coefficients of the series expansions of the stress and displacement fields (2.3) and (2.4) are calculated from the solution of the linear system (3.14) and (3.15), for every assigned value of the contact half-angle α, then, the contact pressure between jaws and disc is given by

$$p(\theta) = -\sigma_{rr}(R, \theta) = \mu \left(A_0 + 2\sum_{n=1}^{N} A_n \cos 2n\theta \right), \tag{3.18}$$

and the resultant of the contact pressure distribution along the loaded rim provides the total load P acting on the disc

$$P = 2Rb \int_0^{\alpha} p(\theta) \cos\theta \, d\theta. \tag{3.19}$$

where b is the disc thickness. The introduction of eqn (3.18) in (3.19) then yields

$$P = 2\mu\, Rb \left(A_0 \sin\alpha + 2\sum_{n=1}^{N} A_n \frac{2n\cos\alpha \sin 2n\alpha - \sin\alpha \cos 2n\alpha}{4n^2 - 1} \right). \tag{3.20}$$

The rigid body displacement $\delta = -u_r(R, 0)$ follows from eqn (2.8) calculated at $\theta = 0$ as

$$\frac{\delta}{R} = -\frac{1-\kappa}{4} A_0 + \sum_{n=1}^{N} \left(\frac{1}{2n-1} + \frac{\kappa}{2n+1} \right) \frac{A_n}{2}. \tag{3.21}$$

By using eqn (2.6), the normal tractions along the loaded diameter of the disc follow from eqn (2.3) calculated at $\theta = 0$ as

$$\frac{\sigma_{rr}(r,0)}{\mu} = -A_0 - 2\sum_{n=1}^{\infty} A_n \left[n \left(\frac{r}{R}\right)^{2(n-1)} - (n-1)\left(\frac{r}{R}\right)^{2n} \right],$$
$$\frac{\sigma_{\theta\theta}(r,0)}{\mu} = -A_0 + 2\sum_{n=1}^{\infty} A_n \left[n \left(\frac{r}{R}\right)^{2(n-1)} - (n+1)\left(\frac{r}{R}\right)^{2n} \right]. \tag{3.22}$$

The pressure distributions along the contact zone is well approximated by the Hertzian pressure distribution given by

$$p_H(\theta) = C\sqrt{\alpha^2 - \theta^2}, \tag{3.23}$$

where the constant C is determined from condition (3.19) for $p = p_H$ as

$$C = \frac{P}{Rb\pi\,\alpha\, J_1(\alpha)}, \tag{3.24}$$

being J_1 the Bessel function of the first kind of order 1.

4. Results

The results presented in the next Section are obtained by considering a number of terms $N = 40$ in the linear algebraic system (3.14)–(3.15). Preliminary tests proved that this number of terms is suitable for obtaining sufficiently accurate results. The following results refer to the ratio $\rho = 2/3$ between the disc and jaw radii adopted by ISRM and to the Poisson ratio $\nu = 0.26$ considered in Ref. 15 for Dionysos marble.

The normalized distributions of the contact pressure p along the contact rim calculated in (3.18) with the angular coordinate θ are plotted in Fig. 2*a* (solid lines), for various angular contact extents. The Hertzian pressure distributions (3.23)–(3.24) for the same applied load and contact angular extent are also plotted in this figure (dashed lines). It can be observed that the contact pressure distributions provided by the present analysis is almost of Hertzian type, also for large values of the applied load, in agreement with the finding of.[16] A small difference from the Hertzian distribution is however observed near the ends of the contact region.

The normalized variation of the applied total load P with the total displacement between the two jaws 2δ plotted in Fig. 2*b* clearly shows that the applied load increases more than linearly with the jaw displacement, due to the advance of the contact length.

The nonlinear variations of the contact angular extent α between jaws and disc with the jaw displacement δ and with the total load P applied to the jaws are then reported in Fig. 3*a* and 3*b*, respectively.

4.1. Stress field within the disc

The tensile tractions and the compressive radial stress along the diameter of the disc laying in the direction of load ($\theta = 0$) are plotted in Fig. 4*a* and 4*b*, respectively, for various angular contact extents. These plots clearly show that the stress field along this diameter is almost uniform only if the contact length is small enough. As the applied load P is increased the contact length increases and the tensile tractions display a clear maximum at the disc centre, where the magnitude of the compressive radial stress attains a minimum. Obviously, the magnitude of both stress components increases with increasing applied load. In particular, the variation of the maximum tensile stress at the disc centre with the applied load or jaw displacement is illustrated in Fig. 5. Interestingly, these results show that the relation between the maximum tensile stress at the disc centre and the jaw displacement is almost linear, and thus a simple approximate relation is proposed, namely

$$\frac{\sigma_{\theta\theta}(0,0)}{\mu} = 0.57\frac{\delta}{R}. \tag{4.1}$$

The following equation that relates the applied load P and half contact angle $\boldsymbol{\alpha}$ with the maximum tensile stress at the centre of the disc is derived in Ref. 4 by assuming uniform contact pressure

CORRECTED PROOF

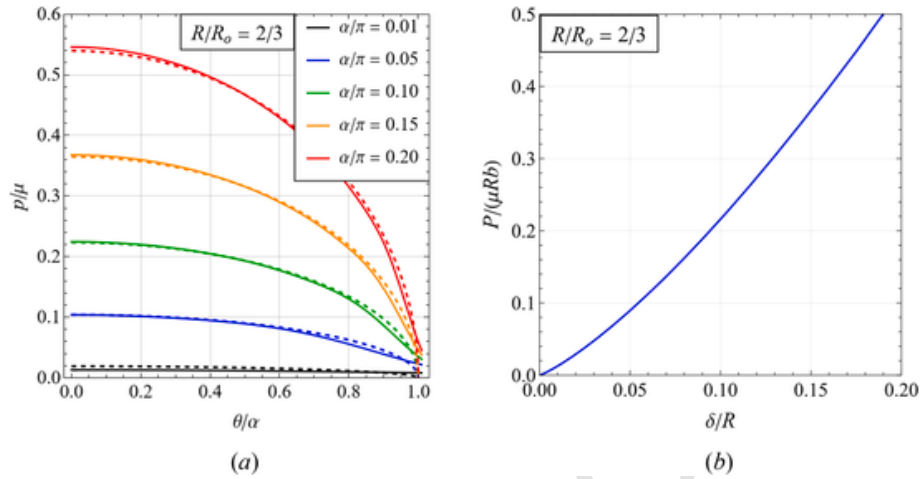


Fig. 2. Normalized distributions of the contact pressure p along the contact rim (solid lines) and of the Hertzian pressure p_H (dashed lines) with the angular coordinate θ for five contact angular extents (a). Normalized variation of the total load P applied to the jaws with the jaw displacement δ (b).

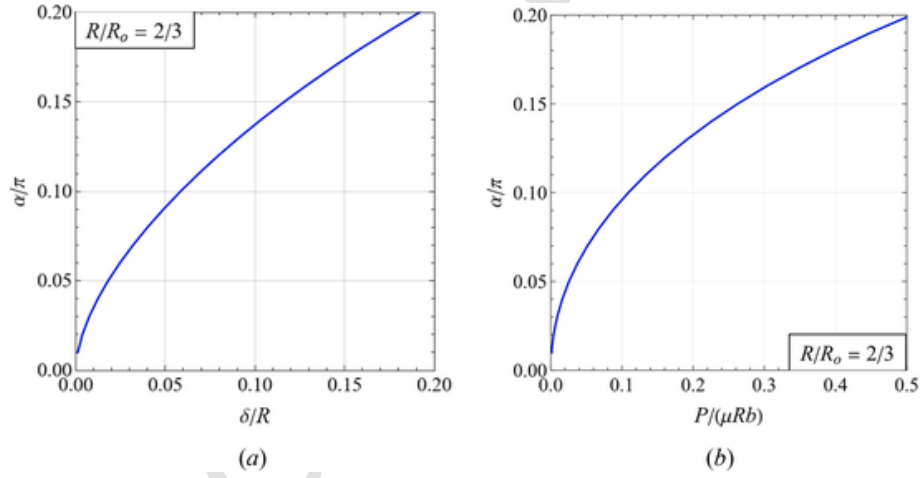


Fig. 3. Normalized variations of the contact angular extent α with the jaw displacement δ (a) and with the total load P applied to the jaws (b).

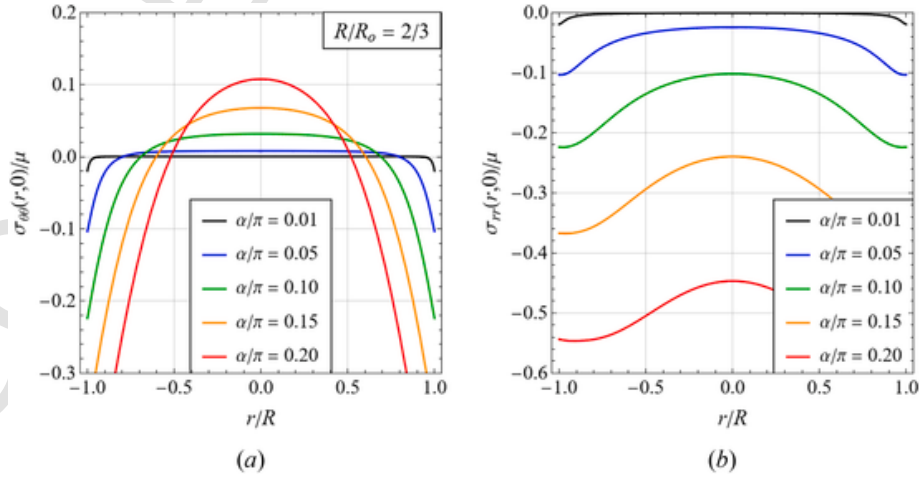


Fig. 4. Normalized variation of the principal stresses along the diameter of the disc laying in the direction of loading (θ = 0). Positive values indicate tension, while negative values represent compression.

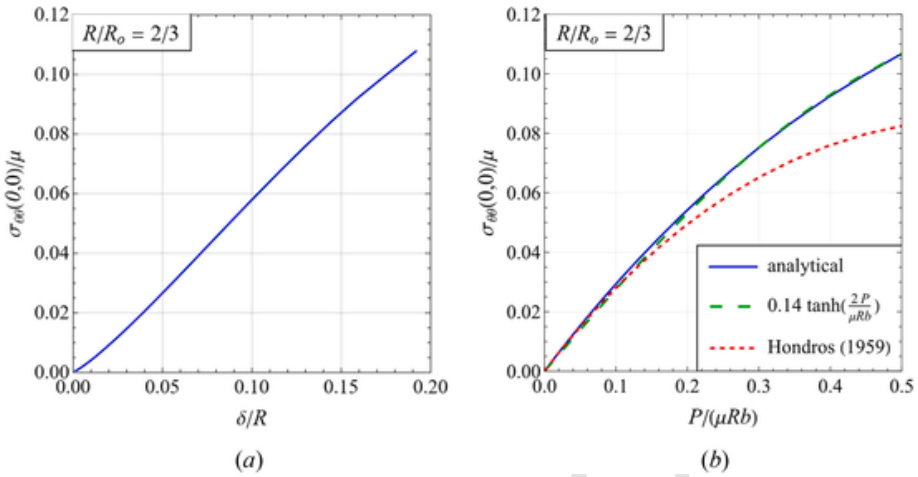


Fig. 5. Normalized variations of the maximum tensile stress at the disc centre with the jaw displacement δ (*a*) and with the total load *P* applied to the jaws (*b*). The red dashed curve corresponds to the predictions in Ref. 4 under a uniform contact pressure. (For interpretation of the references to colour in this figure legend, the reader is referred to the Web version of this article.)

$$\sigma_{\theta\theta}(0,0) = \frac{P}{\pi R b}\frac{\sin 2\alpha - \alpha}{\alpha}. \tag{4.2}$$

Although its validity is questioned,[34] eqn (4.2) is largely employed for calculating the tensile strength of materials from the results of the Brazilian disc test, often by introducing the simplifying assumption $\alpha \to 0$, due to the difficulty of determining the contact angular extent at the onset of cracking at the disc centre. The trend of eqn (4.2) is plotted in Fig. 5*b* and compared with the predictions of the present analysis. As the contact length increases, one can see that the tensile stress predicted by eqn (4.2) (dashed red curve) is significantly lower than that provided by the present approach (solid blue curve). This discrepancy may be due to the uniform distribution of the contact pressure assumed in Ref. 4, or to the assumption of rigid jaws and simplified contact condition $(2.2)_2$ assumed here. The latter condition follows from the exact contact condition (A.5) under the assumption of almost conformal contact, namely for R_0/R approaching 1. Since the ratio R_0/R for the ISMR standard test is 1.5, then the assumption $(2.2)_2$ may result rather inaccurate.

A suitable approximation of the principal tensile stress at the disc centre provided by the present analysis is given by the following relation

$$\sigma_{\theta\theta}(0,0) = 0.14\,\mu\,\tanh\left(\frac{2P}{\mu R b}\right), \tag{4.3}$$

which is also plotted in Fig. 5b (dash-dotted green curve) and turns out to be very close to the analytical results within the range considered in the plot. It must be observed that the tensile stress at the disc centre necessarily depends on the elastic constitutive parameters μ and ν of the disc. Therefore, the Brazilian disc test can efficiently provide the tensile strength of the material, but only if these constitutive parameters are known in advance.

The variation of the ratio between the compressive and tensile principal stresses at the disc centre with the jaw displacement and with the total load applied to the jaws are plotted in Fig. 6a and b, respectively. This ratio is equal to 3 for very small length of the loaded rim and it increases with increasing contact length and thus with increasing applied load or jaw displacement.

4.2. Griffith failure criterion for brittle materials

Generally, the disc failure occurs along the loaded diameter under biaxial stress conditions, namely under compressive radial stress $\sigma_{rr}(r, 0)$ and tensile stress $\sigma_{\theta\theta}(r, 0)$. Therefore, a failure criterion must be adopted for extrapolating the uniaxial tensile strength from a Brazilian

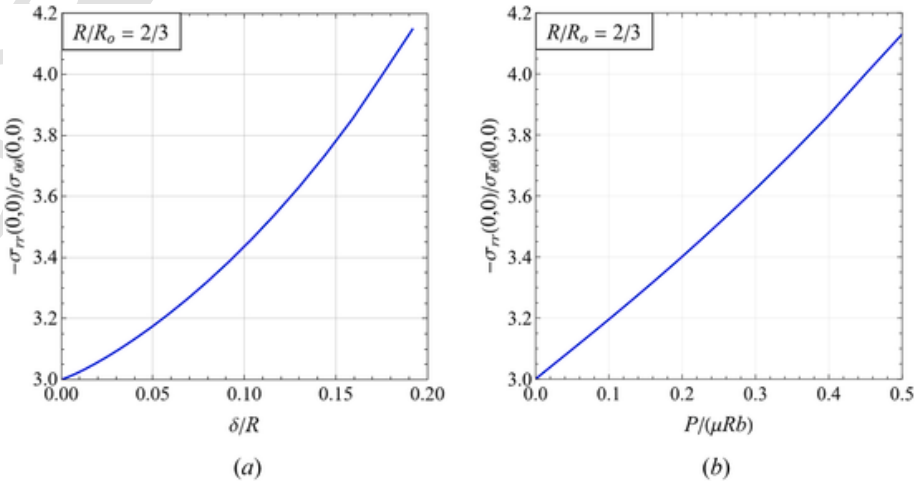


Fig. 6. Variations of the biaxial stress ratio at the disc centre with the jaw displacement δ (*a*) and with the total load *P* applied to the jaws (*b*).

disc test. Usually, the Griffith failure criterion is applied for brittle materials,[34] whereas the von Mises failure criterion is more suitable for ductile material. According to the Griffith failure criterion,[35] crack initiation in rocks occurs when the Griffith equivalent stress

$$\sigma_G = -\frac{(\sigma_{\theta\theta} - \sigma_{rr})^2 + 4\sigma_{r\theta}^2}{8(\sigma_{\theta\theta} + \sigma_{rr})}, \tag{4.4}$$

is greater than or equal to the tensile strength σ_T of the brittle material. For measuring the uniaxial tensile strength of brittle material by means of the Brazilian disc test reliably, it is particularly important that the maximum Griffith equivalent stress be located at the disc centre. The Griffith equivalent stress σ_G at the disc centre also displays an almost linear variation with the jaw displacement δ (see Fig. 7*a*), which can be approximated by the simple relation

$$\frac{\sigma_G(0,0)}{\mu} = 0.6\frac{\delta}{R}, \tag{4.5}$$

whereas its variation with the applied load P, plotted in Fig. 7*b*, is actually nonlinear. The contour plots of the Griffith equivalent stress in Fig. 8 show that its maximum is located there for the two loading levels considered in Fig. 8*a* and *b*, so that the crack will begin there and then propagate towards the edges of the contact rim, as noted also in Refs. 8,36, specially for stiff rocks. Fig. 9 shows that the largest equivalent von Mises stress is attained near the loaded rim when the contact length is small, namely for $\alpha/\pi = 0.1$, and it moves towards the disc centre for large contact length, here for $\alpha/\pi = 0.2$.

5. Validation by comparison with numerical and experimental results

A comparison with the numerical results of the FEM analysis performed in Ref. 37 is then performed for validating the present analytical study. To this aim, the load versus displacement relations predicted by both approaches are plotted in Fig. 10, for a granite disc of radius $R = 25$ mm, thickness $b = 25$ mm, shear modulus $\mu = 17.5$ GPa and Poisson coefficient $\nu = 0.23$, loaded by curved steel jaws denoted by Type III loading configuration in Ref. 37. A reasonably good agreement can be observed in Fig. 10, although the present study (dashed blue line) predicts a slightly larger displacement between the jaws, with respect to the FEM results (orange solid line) under the same applied load. The discrepancy may be due to the assumption of rigid behavior of the jaws made in the present study, whereas in the FEM analysis performed in Ref. 37 the steel jaws display linear elastic behavior, with an elastic Young modulus about five times greater than that of the disc. It follows that, as the applied load increases, the contact length increases faster with respect to the present study due to the jaw elastic deformability and correspondingly the displacement between jaws is smaller. Of course, the present elastic analysis is valid up to the occurring of crack initiation for $P = 24.1$ kN.

A good agreement between analytical and FEM results is also observed for the tensile stress along the loaded diameter of the disc under

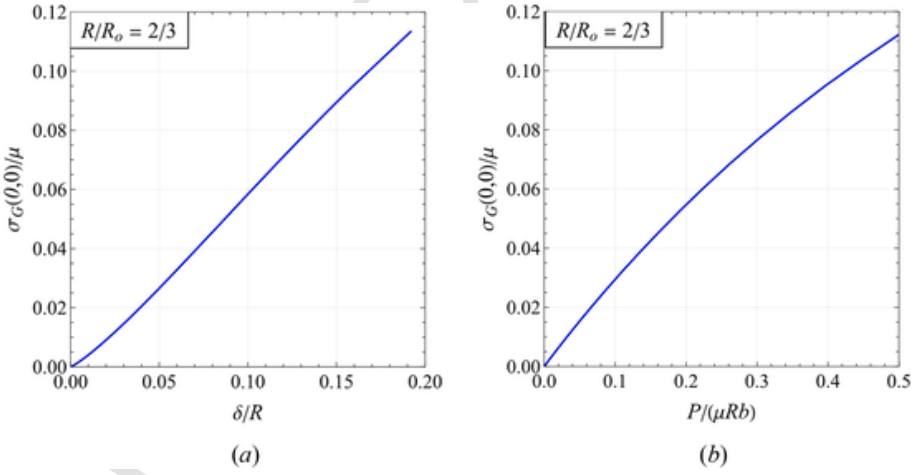


Fig. 7. Normalized variations of the Griffith equivalent stress at the disc centre with the jaw displacement δ (*a*) and with the total load *P* applied to the jaws (*b*).

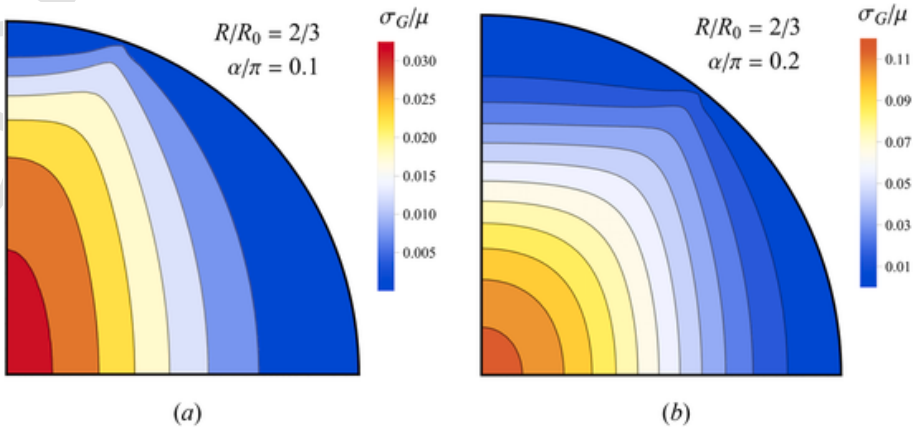


Fig. 8. Contour plots of the normalized Griffith equivalent stress σ_G within a disc quarter for two different loading levels corresponding to the contact angular extents $\alpha/\pi = 0.1$ (*a*) and $\alpha/\pi = 0.2$ (*b*).

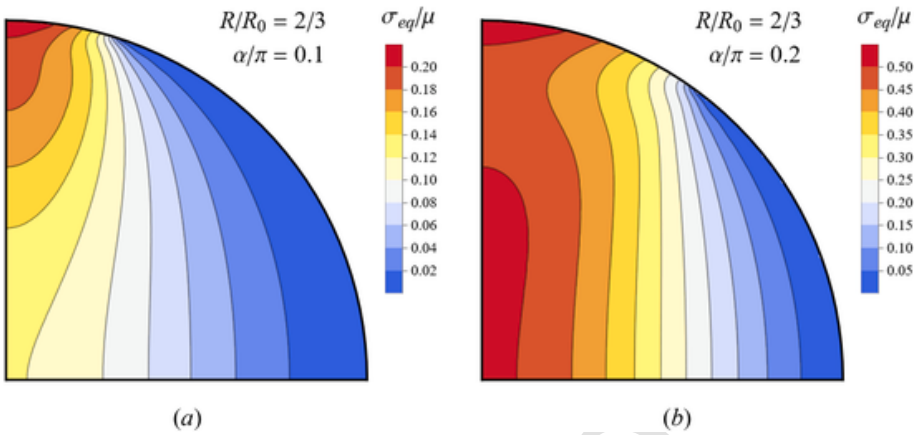


Fig. 9. Contour plots of the normalized von Mises equivalent stress σ_{eq} within a disc quarter for two different loading levels corresponding to the contact angular extents $\alpha/\pi = 0.1$ (*a*) and $\alpha/\pi = 0.2$ (*b*).

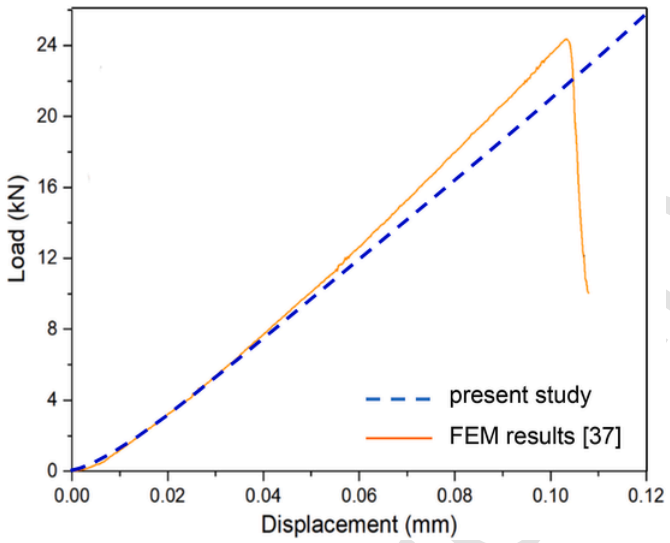


Fig. 10. Comparison between the variations of the applied load P with the total displacement 2δ of a granite disc predicted by the present analysis (dashed line) and by the FEM analysis performed in Ref. 37 (solid line).

the load $P = 10$ kN, plotted in Fig. 11. In this case indeed, the tensile stress is almost constant along the loaded diameter and is equal to 4.96 MPa according to the FEM analysis, whereas the present analytical approach provides 5.35 MPa.

The variation of the half-contact angular extent α with the applied load P predicted by the present study (dashed lines) is compared in Fig. 12 with the numerical results of the FEM analysis performed in Ref. 18 (solid lines) and with the analytical results derived in Ref. 16 (dot-dashed line), for $\nu = 0.38$, $R/R_0 = 2/3$, and for three different elastic moduli of the disc. As expected, the present approach yields a bit smaller contact length due to the simplifying assumption of rigid behavior of the jaws made here, as well as to the approximated boundary condition $(2.2)_2$, which strictly holds for almost conformal contact problems. The contact angle found by the present analysis is a bit underestimated also with respect to the theoretical and experimental results presented in Ref. 16 for a PMMA disc with Young modulus $E = 3.2$ GPa and $\nu = 0.38$, as it may be observed in Fig. 13, where the red dashed line denotes the results of the present approach and the black solid line and the symbols denote the theoretical and experimental results obtained in Ref. 16, respectively.

A comparison between the analytical results obtained here for the strains along the loaded diameter and the experimental and theoretical results provided in Ref. 15 is given in Fig. 14 for a PMMA disc with $\mu = 1.17$ GPa and $\nu = 0.36$. The results plotted in Fig. 14 show that the radial and transverse strains along the loaded diameter predicted by the present approach are a bit smaller in the central part of the disk and larger near the loaded rim with respect to the experimental and theoretical strains provided in Ref. 15.

6. Conclusions

The advancing contact problem occurring in the Brazilian disc test is revisited here by employing a new analytical approach for the determination of the contact pressure and contact angular extent varying the applied load, based on the solution of a dual trigonometric series and validated by comparison with both numerical and experimental results.

For the sake of simplicity, the disc is modelled as a linear elastic material and the jaws are considered as rigid bodies, since the deformation of the metallic jaws is much smaller than that of the rock or concrete disc. The stress and displacement fields in the disc are assumed in the form of a Mitchel series solution, whose coefficients are determined by imposing the frictionless contact boundary conditions. The increase in the contact angular extent with the applied load is then calculated by iterative procedure.

The most important features of the present study are.

- The approach provides explicit closed-form solutions for the full-field stresses in the disc, contact pressure and jaw displacement by considering an advancing contact problem.
- The analytical solution to a mixed boundary value problem is obtained making use of dual trigonometric series.
- The contact conditions for closely conformal contact problem are fulfilled at the lowest order.
- The parametric nature of the study allows for considering any jaw radius and arbitrary elastic constitutive parameters of the disc.
- The contact pressure distribution is found to be almost Hertzian.
- An approximated expression is suggested for the tensile strength under the applied load.

The present analytical investigation confirmed that accounting for advancing contact between disc and jaws yields a nonlinear increase of the applied load with the jaw displacement.

Moreover, the results provided here agree enough well with the predictions of FEM analyses, although a larger displacement between the jaws is found with respect to the FEM results under the same applied load. We must also recognize that the maximum tensile stress origi-

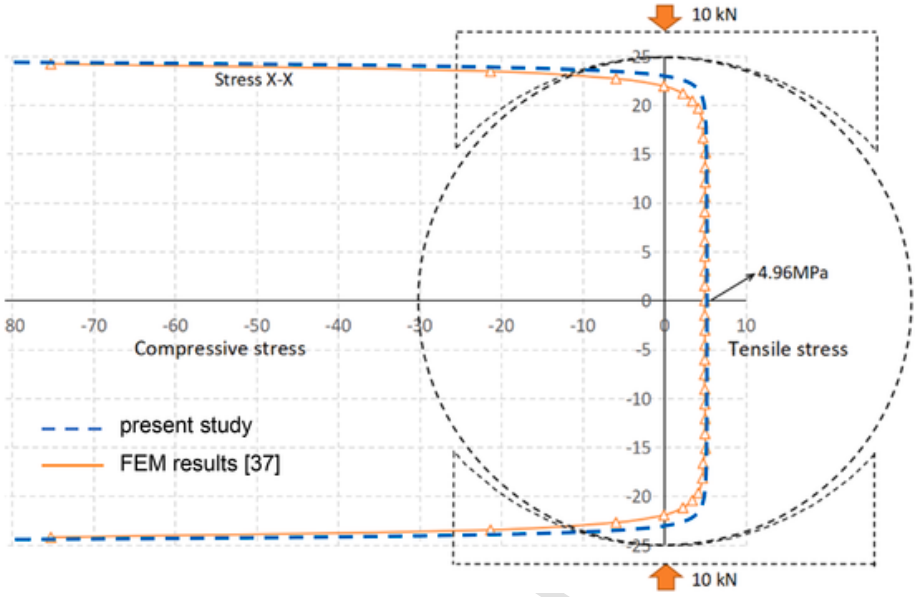


Fig. 11. Comparison between the tensile stress along the loaded diameter of a granite disc under the load $P = 10$ kN predicted by the present analysis (dashed line) and by the FEM analysis performed in Ref. 37 (solid line).

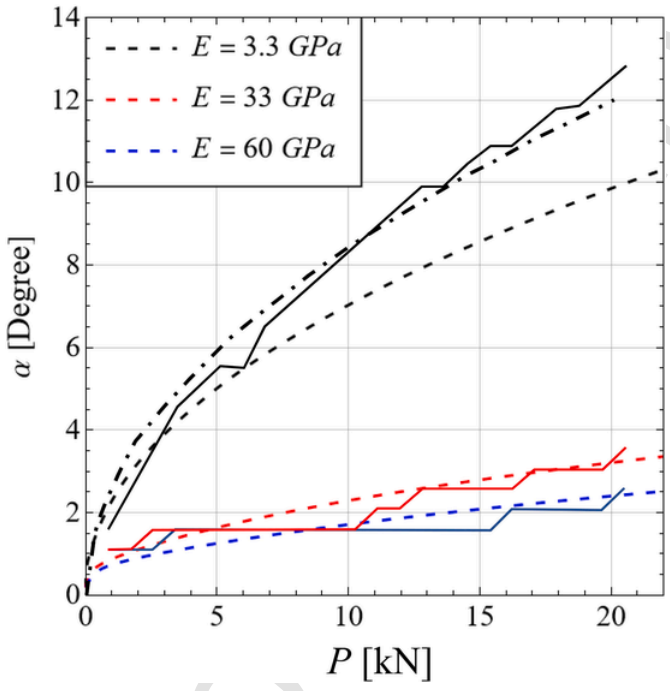


Fig. 12. Relations between the half contact angle α and the total applied load P for an elastic disc predicted by the present analysis (dashed lines), by the FEM analysis performed in Ref. 18 (solid lines) and by the analytical study performed in Ref. 16 (dot-dashed line), for $\nu = 0.38$ and $R/R_0 = 2/3$.

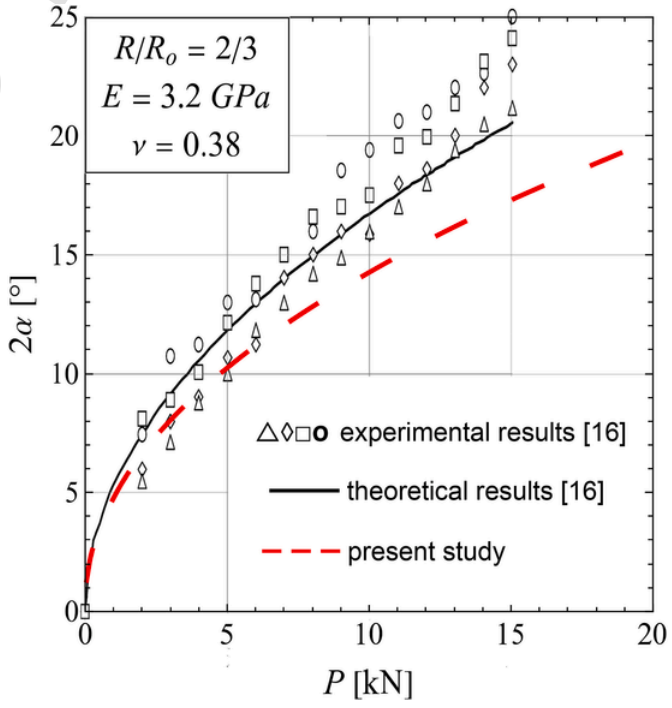


Fig. 13. Variation of the contact angle versus the applied load as determined experimentally following four different approaches in Ref. 16, as calculated analytically in Ref. 16 (black solid line), and as predicted by the present analysis (red dashed line). (For interpretation of the references to colour in this figure legend, the reader is referred to the Web version of this article.)

nated by the applied load P is a bit larger, and the contact angle extent is a bit smaller than that observed in previous numerical and experimental investigations, most probably due to the simplified contact condition here considered. An enhancement of the present investigation according to the exact formulation of the contact condition developed in the Appendix is a work in progress of the author.

Declaration of competing interest

The authors declare that they have no known competing financial interests or personal relationships that could have appeared to influence the work reported in this paper.

Data availability

Data will be made available on request.

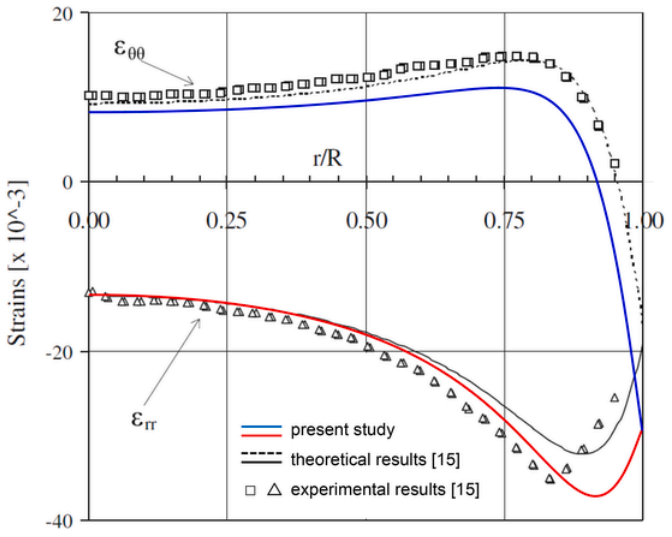


Fig. 14. Experimental measured and theoretical calculated radial and transverse strains along the compressive radius of a PMMA disc subject to the Brazilian disc test according to the ISRM standard, with $\mu = 1.17$ GPa and $\nu = 0.36$. The analytical predictions of the present analysis are denoted by red and blue solid lines, those reported in Ref. 15 by black solid and dashed lines, the experimental results provided in Ref. 15 are marked with squares and triangles. (For interpretation of the references to colour in this figure legend, the reader is referred to the Web version of this article.)

Acknowledgements

Financial support within the framework of the grant MIUR-PRIN2020 "Mathematics for industry 4.0" (code 2020F3NCPX) is gratefully acknowledged.

CORRECTED PROOF

Appendix. Derivation of the contact condition on the displacements

With reference to Fig. A1, where the dotted arc represents the elastic disc rim before the interaction with the jaw and the solid arc denotes the deformed boundary of the disc in contact with the rigid jaw, the displacement vector of a material point along the rim of the disc in contact with the jaw has the following component in the Cartesian coordinate system $(0, x, y)$:

$$\begin{aligned} u_x &= R_0 \sin\psi - R\sin\theta, \\ u_y &= R(1-\cos\theta) - R_0(1-\cos\psi) - \delta, \end{aligned} \tag{A.1}$$

where the angular coordinates θ and ψ are illustrated in Fig. A1, and the following relations hold between the Cartesian and polar components of the displacement vector

$$\begin{aligned} u_x &= u_\theta \cos\theta + u_r \sin\theta, \\ u_y &= -u_\theta \sin\theta + u_r \cos\theta. \end{aligned} \tag{A.2}$$

being u_r and u_θ the displacement components in the polar coordinate system $(0, r, \theta)$. By comparing eqns (A.1) and (A.2) one obtains

$$\begin{aligned} R_0 \sin\psi &= u_\theta \cos\theta + (R + u_r)\sin\theta, \\ R_0 \cos\psi &= R_0 - R + \delta - u_\theta \sin\theta + (R + u_r)\cos\theta, \end{aligned} \tag{A.3}$$

and, thus, squaring both eqns and then summing, one has

$$\begin{aligned} &u_\theta^2 + (R+u_r)^2 + (R-\delta)^2 - 2R_0(R-\delta) \\ &\quad + 2\,(R_0 - R + \delta)\left[(R+u_r)\cos\theta - u_\theta \sin\theta\right] = 0. \end{aligned} \tag{A.4}$$

Under the hypothesis of infinitesimal displacement, one can assume that u_r, u_θ and δ are much smaller than R and R_0. Therefore, by neglecting the quadratic terms in these small quantities, from eqn (A.4) one gets

$$\begin{aligned} \frac{u_r}{R} = \left(\frac{R_0}{R} - 1\right)\left(1 - \cos\theta - \frac{\delta}{R} - \frac{u_r}{R}\cos\theta + \frac{u_\theta}{R}\sin\theta\right) \\ - \frac{\delta}{R}\cos\theta. \end{aligned} \tag{A.5}$$

If the terms u_r/R, u_θ/R, and δ/R are neglected with respect to $1-\cos\theta$, then eqn (A.5) reduces to eqn $(2.2)_2$, namely

$$\frac{u_r}{R} = \left(\frac{R_0}{R} - 1\right)(1 - \cos\theta) - \frac{\delta}{R}\cos\theta. \tag{A.6}$$

Eqn (A.6) was derived in Ref. 20 and later in Refs. 28,29 for almost conformal contact problems, namely for $R_0/R = 1 + \varepsilon$, where $0 < \varepsilon \ll 1$. For low conformal contact problems, eqn (A.6) is just approximated and the exact contact condition is given by eqn (A.5) instead.

For straight jaws like those adopted by the ASTM the radius R_0 tends to infinity and thus from eqn (A.5) the following contact condition is obtained

$$\frac{u_r}{R}\cos\theta - \frac{u_\theta}{R}\sin\theta = 1 - \frac{\delta}{R} - \cos\theta. \tag{A.7}$$

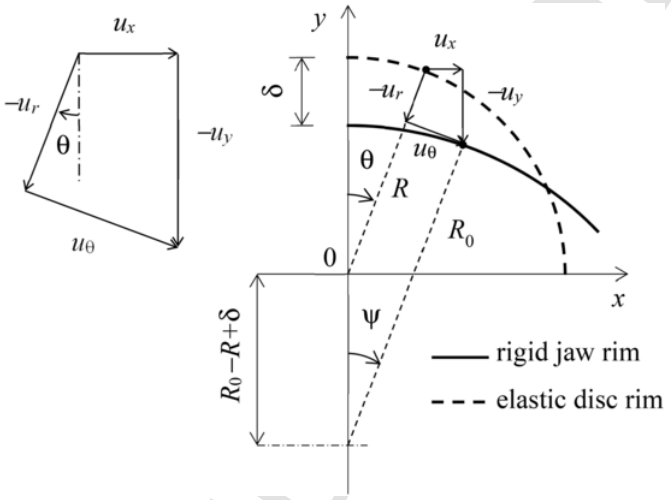


Fig. A1. Displacement of a material point along the rim of the disc in contact with the upper jaw.

References

1. Ouchterlony F. Suggested methods for determining the fracture toughness of rock. *Int J Rock Mech Min Sci.* 1988;25(2):71–96.
2. Li D., Wong L.N.Y. The Brazilian disc test for rock mechanics applications: review and new insights. *Rock Mech Rock Eng.* 2013;46:269–287.
3. Muskelishvili N.I. *Some Basic Problem of the Mathematical Theory of Elasticity*. Groningen: Noordhoff; 1963.
4. Hondros G. The evaluation of Poisson's ratio and the modulus of materials of a low tensile resistance by the Brazilian (indirect tensile) test with particular reference to concrete. *Aust J Appl Sci.* 1959;10:243–268.
5. Fairhurst C. On the validity of the 'Brazilian' test for brittle materials. *Int J Rock Mech Min Sci.* 1964;1:535–546.
6. Jianhong Y., Wu F.Q., Sun J.Z. Estimation of the tensile elastic modulus using Brazilian disc by applying diametrically opposed concentrated loads. *Int J Rock Mech Min Sci.* 2009;46(3):568–576.
7. Ma C.C., Hung K.M. Exact full-field analysis of strain and displacement for circular disks subjected to partially distributed compressions. *Int J Mech Sci.* 2008;50 (2):275–292.
8. Erarslan N., Liang Z.Z., Williams D.J. Experimental and numerical studies on determination of indirect tensile strength of rocks. *Rock Mech Rock Eng.* 2012;45: 739–751.
9. Kourkoulis S.K., Markides C.F., Chatzistergos P.E. The Brazilian disc under parabolically varying load: theoretical and experimental study of the displacement field. *Int J Solid Struct.* 2012;49(7–8):959–972.
10. Kourkoulis S.K., Markides C.F. Stresses and displacements in a circular ring under parabolic diametral compression. *Int J Rock Mech Min Sci.* 2014;71:272–292.
11. Garcia-Fernandez C.C., Gonzalez-Nicieza C., Alvarez-Fernandez M.I., Gutierrez-Moizant R.A. Analytical and experimental study of failure onset during a Brazilian test. *Int J Rock Mech Min Sci.* 2018;103:254–265.
12. Yu J., Shang X., Wu P. Influence of pressure distribution and friction on determining mechanical properties in the Brazilian test: theory and experiment. *Int J Solid Struct.* 2019;161:11–22.
13. Gutiérrez-Moizant R., Ramírez-Berasategui M., Santos-Cuadros S., García-Fernández C.C. A novel analytical solution for the Brazilian test with loading arcs. *Math Probl Eng.* 2020;2935812:1–19.
14. Lu A., Wang S., Cai H. Closed-form solution for the stresses in Brazilian disc tests under vertical uniform loads. *Rock Mech Rock Eng.* 2018;51:3489–3503.
15. Markides C.F., Kourkoulis S.K. The stress field in a standardized Brazilian disc: the influence of the loading type acting on the actual contact length. *Rock Mech Rock Eng.* 2012;45(2):145–158.
16. Kourkoulis S.K., Markides C.F., Chatzistergos P.E. The standardized Brazilian disc test as a contact problem. *Int J Rock Mech Min Sci.* 2013;57:132–141.
17. Markides C.F., Kourkoulis S.K. The influence of jaw's curvature on the results of the Brazilian disc test. *J Rock Mech Geotech Eng.* 2016;8(2):127–146.
18. Yuan R., Shen B. Numerical modelling of the contact condition of a Brazilian disc test and its influence on the tensile strength of rock. *Int J Rock Mech Min Sci.* 2017; 93:54–65.
19. Barber J.R. *Contact Mechanics*. Berlin: Springer International Publishing; 2018.
20. Persson A. *On the Stress Distribution of Cylindrical Elastic Bodies in Contact*. Sweden: Chalmers University; 1964. PhD Dissertation.
21. Rao A.K. Elastic analysis of pin joints. *Compos Struct.* 1978;9:125–144.
22. Ciavarella M., Decuzzi P. The state of stress induced by the plane frictionless cylindrical contact. I. The case of elastic similarity. *Int J Solid Struct.* 2001;38 (26–27):4507–4523.
23. Liu C.S., Zhang K., Yang R. The FEM analysis and approximate model for cylindrical joints with clearances. *Mech Mach Theor.* 2007;42(2):183–197.
24. Radi E., Strozzi A. Advancing contact of an elastic curved beam indented by a rigid pin with clearance. *Int J Non Lin Mech.* 2023;149:104313.
25. Block J.M., Keer L.M. Partial contact of an elastic coated cylinder pressed by a rigid flat surface. *J Tribol.* 2007;129(1):60–64.
26. Noble B., Hussain M.A. Exact solution of certain dual series for indentation and inclusion problems. *Int J Eng Sci.* 1969;7(11):1149–1161.
27. Yu J., Shang X., Wang G. Theoretical analysis and experimental identification of contact pressure in Brazilian disc. *Rock Mech Rock Eng.* 2022;55:799–811.
28. Johnson K.L. *Contact Mechanics*. Cambridge, UK: Cambridge University Press; 1985.
29. Hou J.P., Hills D.A. Contact between a pin and a plate with a hole under interference-fit and clearance-fit conditions. *Proc Inst Mech Eng Part C: J Mech Eng Sci* 2001;215(6):629–639.
30. Barber J.R. *Elasticity*. Dordrecht: Springer; 2010.
31. Omar T., Hassan H.A. Approximate solution for an indentation problem using dual series equations. *Int J Eng Sci.* 1991;29(2):187–194.
32. Dundurs J., Tsai K.C., Keer L.M. Contact between elastic bodies with wavy surfaces. *J Elasticity*. 1973;3:109–115.
33. Sneddon I.N. *Mixed Boundary Value Problems in Potential Theory*. New York, NY: John Wiley; 1966.
34. Navidtehrani Y., Betegón C., Zimmerman R.W., Martínez-Pañeda E. Griffith-based analysis of crack initiation location in a Brazilian test. *Int J Rock Mech Min Sci.* 2022;159:105227.
35. Jaeger J., Cook N.G., Zimmerman R. *Fundamentals of Rock Mechanics*. fourth ed. Oxford, UK: Blackwell Publishing; 2007.
36. Komurlu E., Kesimal A. Evaluation of indirect tensile strength of rocks using different types of jaws. *Rock Mech Rock Eng.* 2015;48(4):1723–1730.

UNCORRECTED PROOF

37. Xiao P., Zhao G., Liu H. Failure transition and validity of Brazilian disc test under different loading configurations: a numerical study. *Math.* 2022;10(15):2681.

CORRECTED PROOF